Differing Adsorption Behavior of Environmentally Important Cyanophenol Isomers at the Air−Water Interface

Melissa C. Kido Soule, Dennis K. Hore, Donna M. Jaramillo-Fellin,† and Geraldine L. Richmond*

Department of Chemistry, University of Oregon, 1253 University of Oregon, Eugene, Oregon 97403

Received: March 3, 2006; In Final Form: May 12, 2006

Vibrational sum-frequency spectroscopy and surface tensiometry have been used to study the adsorption of *m*- and *p*-cyanophenol at the air−water interface. Spectra of the cyano (CN) group under different polarization schemes are utilized to determine its hydrogen bonding environment and orientation. For both isomers, it is found that the cyano group is hydrogen bonded at the interface but that the CN orientation is independent of surface density. The average CN tilt angle (θ_0), however, is found to differ between the isomers, such that the CN group points down toward the aqueous phase for *m*-cyanophenol ($\theta_0 = 96-106°$) but points up toward the vapor phase for the *p*-cyanophenol ($\theta_0 = 65-80°$). In addition, this average tilt angle is distributed over a narrow range, $\sigma_0 < 10°$ for the meta isomer and $\sigma_0 < 16°$ for the para isomer.

Introduction

Aqueous surfaces and interfaces play a significant role in a wide variety of environmental processes, from heterogeneous atmospheric chemistry to the transport of materials through soils. Evidence suggests, for example, that the vapor-water interface in soils may serve as an important domain for the retention of organic species.[1] Understanding the surface reactivity of these species is critical to the prediction of migration rates of contaminants through soil−water systems.[2] Organic molecules emitted into the atmosphere can partition between the gas and liquid phases of atmospheric aerosols and react with atmospheric oxidants such as O_3 and OH.[3−5] Investigations into how organic species adsorb and orient at the aqueous interface are necessary to better understand the role of aerosols in areas such as heterogeneous reaction chemistry and cloud formation dynamics.

Phenols such as cyanophenols are an important class of organic molecules that persist in the environment because derivatives of these compounds are widely used as bactericides and pesticides.[6] Bromoxynil (3,5-dibromo-4-hydroxybenzonitrile) and other halo-cyanophenol pesticides have been detected in rain samples and in the gas phase.[7] The main abiotic degradation pathways for these pesticides are photolysis by direct irradiation of sunlight, oxidative reactions with OH or nitrate radicals, and hydrolysis.[7,8] Results from a recent molecular dynamics study indicate that oxidants such as OH exhibit a propensity for the air−water interface.[9] This is particularly relevant to the case of cyanophenol-derived pesticides which can adsorb to the liquid aerosol surface and be potentially oxidized, providing a mechanism for conversion or removal. Understanding the importance of such a mechanism requires a detailed knowledge of the behavior of cyanophenol species at the air−water interface.

Much experimental work has been carried out to understand the properties of cyanophenol. Its general toxicity has been examined repeatedly, including a recent study of dermal absorption from aqueous solutions of *m*-and *p*-cyanophenol.[10] In addition, various laboratory studies summarized by Georgieva et al. have probed the hydroxy (ν_{OH}) and cyano (ν_{CN}) stretching modes to investigate hydrogen bonding and complexes of cyanophenol with various Lewis bases.[6] These studies, however, elucidate only the behavior of cyanophenol in bulk solution. Current interfacial data available for cyanophenol are largely thermodynamic, involving surface tension and surface potential measurements that reveal macroscopic properties of the aqueous system.[11] By contrast, vibrational sum-frequency spectroscopy (VSFS) is uniquely ideal for probing interfacial structure at the molecular level. This nonlinear technique is inherently surface-selective because of the naturally occurring breakdown of inversion symmetry at interfaces.[12−14]

Vibrational sum-frequency spectroscopy has been widely used to examine the orientation and conformation of surfactant molecules at the vapor-aqueous interface.[15−17] Such studies have contributed significantly to our understanding of how the interplay between hydrophobic and hydrophilic portions of a solute molecule affects its adsorption and orientation at an interface. For a solute such as *p*-cyanophenol, however, where both CN and OH aromatic substituents can participate in hydrogen bonding, there is less distinction between hydrophobic and hydrophilic regions of the molecule. In this paper, surface tension measurements and vibrational sum-frequency spectroscopy are used to probe the adsorption and orientation of both meta and para isomers of cyanophenol at the air−water interface. The stretching vibration of the cyano group is used to determine both the hydrogen bonding interactions and the average orientation of cyanophenol molecules at the air−water interface. Comparisons are made between *m*- and *p*- cyanophenol to elucidate the effect of aromatic substitution differences on the adsorptive behavior of these compounds. In the first sections of the paper we provide a brief background of the sum-frequency experiment, followed by a description of our results. We then describe how our results are analyzed to reveal the orientation of the cyano group. Our analysis shows that the orientation of

* To whom correspondence should be addressed. E-mail: richmond@uoregon.edu. Phone: 541-346-4635. Fax: 541-346-5859.

† Current address: School of Natural Sciences, University of California, Merced, P.O. Box 2039, Merced, CA 95344.

10.1021/jp061351o CCC: $33.50
Published on Web 07/29/2006

m- and *p*-cyanophenol is invariant to changes in surface number density and that the CN moiety of these isomers adopts different average orientations at the air−water interface.

2. Vibrational Sum-Frequency Spectroscopy: Background

When two intense electric fields of frequencies ω_1 and ω_2 are spatially and temporally overlapped at the interface between two media, they induce a nonlinear polarization in the medium that radiates at the sum of the incident frequencies, $\omega_{SFG} = \omega_1 + \omega_2$. This second-order nonlinear optical phenomenon is called sum-frequency generation (SFG). While SFG is forbidden in media with inversion symmetry, it is allowed at interfaces where inversion symmetry is broken. This principle forms the basis of vibrational sum-frequency spectroscopy (VSFS), in which the vibrational spectrum of an interface is obtained by mixing tunable IR with fixed frequency visible light.

Intensity in the VSFS spectrum is determined by the effective surface second-order susceptibility, $\chi_{eff}^{(2)}$, and the intensities of the incident visible and IR beams:

$$I(\omega_{SFG}) \propto |P^{(2)}(\omega)|^2 \propto |\chi_{eff}^{(2)}|^2 I(\omega_{vis}) I(\omega_{IR}) \quad (1)$$

The effective susceptibility $\chi_{eff}^{(2)}$ is related to the true second-order susceptibility by Fresnel factors $L(\omega)$ and unit polarization vectors $\hat{\mathbf{e}}(\omega)$ for each beam:

$$\chi_{eff}^{(2)} = [\hat{\mathbf{e}}(\omega_{SFG}) \cdot L(\omega_{SFG})] \cdot \chi^{(2)} : [L(\omega_{vis}) \cdot \hat{\mathbf{e}}(\omega_{vis})][L(\omega_{IR}) \cdot \hat{\mathbf{e}}(\omega_{IR})] \quad (2)$$

The second-order susceptibility $\chi^{(2)}$ can be expressed as the sum of a nonresonant component, $\chi_{NR}^{(2)}$, and a resonant component for each vibrational mode ν, $\chi_{R\nu}^{(2)}$.

$$\chi^{(2)} = \chi_{NR}^{(2)} + \sum_{\nu} \chi_{R\nu}^{(2)} \quad (3)$$

In general, both $\chi_{NR}^{(2)}$ and $\chi_{R\nu}^{(2)}$ are complex quantities, and their relative phases must be taken into account. In these studies we assume that ω_{vis} is far enough from any electronic transitions that the nonresonant component can be treated as purely real.

Assuming a Lorentzian distribution of vibrational energies, each vibrational transition can be represented as

$$\chi_{R\nu}^{(2)} = \frac{A_\nu}{\omega_\nu - \omega_{IR} - i\Gamma_\nu} \quad (4)$$

where A_ν, ω_ν, and Γ_ν are fit parameters that denote the strength, resonant frequency, and damping constant of the νth vibrational mode, respectively.[18] This macroscopic resonant susceptibility is related to the molecular hyperpolarizability β through the expression

$$\chi_{R\nu}^{(2)} = \frac{N}{\epsilon_o} \langle \beta_\nu \rangle \quad (5)$$

where N is the surface number density, ϵ_o is the vacuum permittivity, and the angular brackets denote an average over molecular orientations. It is thus possible to determine the average orientation of molecules at the surface by relating the macroscopic susceptibility $\chi^{(2)}$ to the hyperpolarizability β.[19] This process will be discussed in detail in a later section.

Since the surface of a liquid such as water is azimuthally isotropic, only 4 of the 27 elements of $\chi^{(2)}$ are nonzero and unique. With the lab coordinates chosen so that *z* lies along the surface normal and the *xz*-plane is the plane of incidence, they are $\chi^{(2)}_{xxz} = \chi^{(2)}_{yyz}$, $\chi^{(2)}_{xzx} = \chi^{(2)}_{yzy}$, $\chi^{(2)}_{zxx} = \chi^{(2)}_{zyy}$, and $\chi^{(2)}_{zzz}$. In addition, if ω_{vis} is far from resonance, this leaves only three nonzero independent elements of $\chi^{(2)}$, such that $\chi^{(2)}_{xzx} = \chi^{(2)}_{yzy} = \chi^{(2)}_{zxx} = \chi^{(2)}_{zyy}$. These elements can be probed using combinations of incident and outgoing linearly polarized light, namely: ssp, sps (or pss), and ppp, where the letters represent light polarized parallel to the plane of incidence (p) or perpendicular to the plane of incidence (s). All polarization schemes are given in the format sum-frequency, visible, infrared.

3. Experimental Section

Surface Tension. All surface tension measurements were made using the Wilhelmy plate method.[20] The platinum plate was cleaned with a solution of concentrated sulfuric acid containing NoChromix, rinsed with 18 MΩ water from a Nanopure filtration system, and then flamed until glowing before each surface tension measurement. At least six measurements were averaged at each solution concentration. All measurements were made at 295 K.

3.2. Broad-Bandwidth Sum-Frequency Generation (BBSFG) Laser System. Experiments at the vapor/water interface were conducted using a broad-bandwidth sum-frequency generation (BBSFG) laser system built in our laboratory and modeled after the first such system developed in 1998 by Richter et al.[21] In this scheme, a femtosecond IR beam and a picosecond visible beam are coupled spatially and temporally at an interface to generate a third beam at the sum of the two incident frequencies. Like the IR, the sum-frequency has a broad bandwidth, and so the resolution of the experiment is limited by the bandwidth of the visible light.

The BBSFG laser system consists of a home-built Ti:sapphire oscillator that generates 100 fs pulses at 800 nm. These pulses are amplified to 1 mJ/pulse in a 1 kHz Ti:sapphire regenerative amplifier (Spectra Physics, Spitfire) pumped by a Nd:YLF laser (Spectra Physics, Evolution). Approximately 15% of the amplified energy is spectrally narrowed with a grating-aperture assembly to yield ∼2 ps pulses with ∼15 cm^{-1} bandwidth and ∼20 μJ energy. The remainder of the amplified pulse is used to pump an optical parametric amplifier (Spectra Physics, OPA 800C) that produces nominally 100 fs pulses tunable from 3 to 10 μm, with energies per pulse ranging from 12 to 2 μJ. In the present studies, the OPA was tuned to the CN stretching region ∼2240 cm^{-1} where the IR energy was typically 12 μJ per pulse with a bandwidth of ∼175 cm^{-1}.

The femtosecond IR and visible pulses were overlapped in copropagating, external reflection geometry at the interface, with angles from the surface normal of 60° and 45° for the visible and IR, respectively; the detection angle was set to ∼32°. The generated sum-frequency light was spatially and spectrally filtered and dispersed in a spectrometer (Acton, SP150) by a 1200 g/mm diffraction grating blazed at 500 nm. This dispersed light was then collected with a liquid nitrogen cooled CCD camera (Princeton Instruments, 512 × 512 back-illuminated array). BBSFG spectra were obtained by integrating the signal on the CCD for 10−20 min depending on the experiment. These spectra were normalized with the nonresonant BBSFG spectrum from an amorphous gold surface. For these studies, the prominent feature at 2350 cm^{-1} in the nonresonant gold spectrum due to CO_2 vapor absorption was used as a calibration reference. The error in calibrating the IR frequency is ±3 cm^{-1}. An average of at least four spectra for each solution concentration and polarization scheme is presented here, taken over a period of several days to confirm reproducibility. The SFG

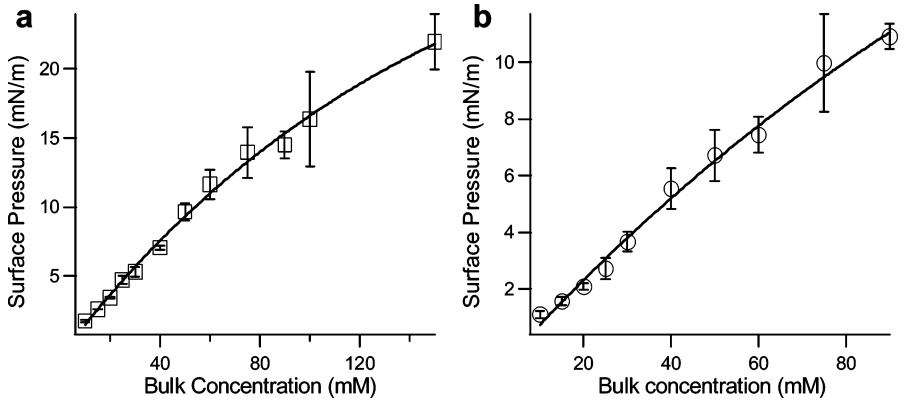

Figure 1. Surface pressure isotherms of (a) *m*-cyanophenol and (b) *p*-cyanophenol at 295 K. The solid lines are fits to the Gibbs isotherm.

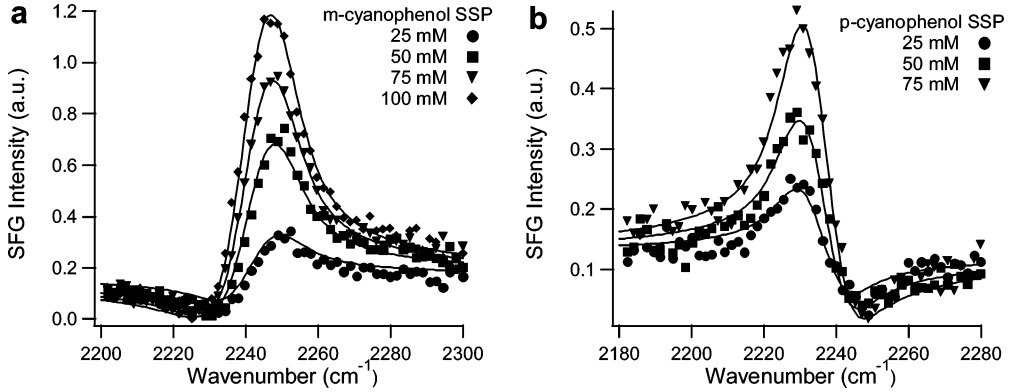

Figure 2. SFG spectra of the CN stretching vibration at different bulk concentrations of (a) *m*-cyanophenol and (b) *p*-cyanophenol using the ssp polarization combination. Solid lines shown are fits to the data.

amplitude error bars are the standard deviations obtained from independently fitting data sets acquired on different days.

Spectral Fitting. Following normalization and calibration, the BBSFG spectra were fit to a line shape that accounted for the effects of homogeneous broadening (Lorentzian line shape) and inhomogeneous broadening (Gaussian line shape) because of the multitude of environments present in the condensed phase[22−24]

$$|\chi^{(2)}(\omega_{SFG})|^{(2)} = |\chi_{NR}{}^{(2)} + \int_{-\infty}^{\infty} \frac{A_\nu}{\omega_L - \omega_{IR} - i\Gamma_L} \exp\left[-\frac{(\omega_L - \omega_\nu)^2}{\Gamma_\nu{}^2}\right] d\omega_L|^2 \quad (6)$$

In this expression A_ν is the resonant amplitude, ω_ν is the resonant frequency, Γ_L and Γ_ν are the homogeneous and inhomogeneous line widths, and ω_L is a variable over which the integral is evaluated.

Sample Preparation. *m*-Cyanophenol (Aldrich, 99%) and *p*-cyanophenol (Acros Organics, 99%) were used as received without further purification. Aqueous solutions were prepared using water from an 18 MΩ Nanopure system. All glassware were cleaned with a H_2SO_4/NoChromix solution followed by copious rinses with Nanopure water.

4. Experimental Results and Analysis.

4.1. Surface Tension. *m*-Cyanophenol (*m*-CP) and *p*-cyanophenol (*p*-CP) display mild surface activity as shown by their surface pressure isotherms in Figure 1. To determine the limiting (maximum) surface concentration, these surface pressure isotherms are fit to the Gibbs equation:[25]

$$\Gamma_i = \frac{1}{RT}\left(\frac{\partial \pi}{\partial \ln a_i}\right)_T \quad (7)$$

where Γ_i is the surface excess concentration at maximum surface coverage, π is the interfacial pressure in mN/m, and a_i is the activity. For dilute solutions, the activity can be replaced by the bulk concentration, C_i. The surface excess coverage for any bulk concentration can then be obtained through the maximum surface excess concentration Γ_i and the Frumkin isotherm:

$$\pi_2 = -\Gamma_i \ln\left[1 - \frac{\Gamma_2}{\Gamma_i}\right] \quad (8)$$

where the subscript 2 indicates the surface pressure or surface excess at a specific bulk concentration. The maximum surface excess concentrations of *m*-CP and *p*-CP obtained from the Gibbs equation are 2.0×10^{14} molecules/cm^2 and 1.5×10^{14} molecules/cm^2, respectively. Thus, according to eq 8, the surface area per molecule of a 75 mM *m*-CP solution is 56 Å^2 (1.8×10^{14} molecules/cm^2), whereas for a 75 mM *p*-CP solution, the surface area per molecule is 76 Å^2 (1.3×10^{14} molecules/cm^2). If the surface area of water and cyanophenol are estimated as 8 Å^2 and 30 Å^2 respectively, then at the interface of a 75 mM solution there are ∼3 water molecules per *m*-CP molecule and ∼5 to 6 water molecules per *p*-CP molecule.[26−28]

4.2. Spectroscopic Studies. Figure 2 shows BBSFG spectra in ssp polarization over a range of concentrations, from 25 to 100 mM for *m*-CP and from 25 to 75 mM for *p*-CP. Aqueous solubility limits determined the maximum concentration studied for both isomers. Only one resonant feature is seen in the spectra corresponding to the symmetric stretch of the cyano group. The distinct peak asymmetry is characteristic of interference between a single resonant peak and the nonresonant background. Each

TABLE 1: Experimental Vibrational Frequencies for the CN Stretching Mode in Various Hydrogen Bonding Environments

	m-cyanophenol (cm^{-1})	*p*-cyanophenol (cm^{-1})
IR ($CHCl_3$)[a]	2234	2226
Raman (H_2O)[b]	2239	2229
Raman (solid)[b]	2244	2233
BBSFG	2242 ± 3	2235 ± 3

[a] Reference 37. [b] Reference 38.

isomer concentration series was fit globally using eq 6 in order to constrain the fitting parameters. In both cases, the Lorentzian width was set to 2 cm^{-1}, the nonresonant background was constrained to be real, and the phase relationship between the resonant and nonresonant components was allowed to have a value of either 180° or 0°. The remaining model parameters were allowed to vary to obtain the best agreement with the data.

Spectral fitting places the CN resonant frequency at 2242 ± 3 cm^{-1} for *m*-CP and 2234 ± 3 cm^{-1} for *p*-CP. That the CN stretching frequency of the para isomer is a bit lower than that of the meta isomer can be understood in terms of the OH/CN polar resonance in *p*-CP.[6,29] A number of studies have shown that the frequency of the CN stretching mode of nitriles, ν_{CN}, is sensitive to solvent environment. For example, ν_{CN} shifts to higher frequency as a result of hydrogen bonding via the nitrogen atom to proton donors such as water.[30−34] The frequency of the CN stretching mode depends on the electron density available to the CN group, with lower electron density generally producing a stronger CN bond with higher vibrational frequency.[32,35,36] This sensitivity provides insight into the hydrogen bonding environment of *m*- and *p*-cyanophenol at the air−water interface.

Infrared and Raman frequencies of the CN mode in different environments are shown in Table 1 for comparison with those obtained from the BBSFG experiments. In $CHCl_3$, the cyano frequencies for *m*-CP and *p*-CP are ~8 cm^{-1} lower than in the solid state.[37,38] This difference can be understood in terms of hydrogen bonding to the CN group that is absent in the case of $CHCl_3$ but present in the solid state. In the solid state, *p*-cyanophenol exists as intermolecularly hydrogen bonded chains involving O−H···N bonds to the CN group.[6,39] X-ray crystallography also reveals that, like the para isomer, the solid state of the ortho isomer is characterized by chains of molecules connected through O−H···N hydrogen bonds. Given the structural similarities between the isomers, it is reasonable that the meta isomer also exists in the solid state as extended chains of intermolecularly hydrogen-bonded molecules. In bulk aqueous solutions of *m*-CP and *p*-CP, the CN stretching frequencies are also blue-shifted from the $CHCl_3$ case, indicating hydrogen bonding to the CN group. Thus, comparison between the BBSFG ν_{CN} and the bulk aqueous and solid CN stretching frequencies in Table 1 clearly shows that the CN groups of *m*-CP and *p*-CP are hydrogen bonded at the aqueous interface.

Although it is clear that the cyano groups are hydrogen bonded at the air−water interface, there remains some ambiguity as to whether cyanophenol is interacting with water or with another cyanophenol molecule (i.e., dimerization). Support for hydrogen bonding interactions with water comes from the observation that ν_{CN} does not change over the range of bulk concentrations studied, yet the surface water-to-cyanophenol ratio increases significantly between the 75 and 25 mM solutions. For example, at the surface of a 75 mM solution, there are ~3 water molecules per *m*-CP, while for a 25 mM solution there are ~10 water molecules per *m*-CP (~106 $Å^2$/molecule). The likelihood of water-cyanophenol interactions is therefore higher at the surface of a 25 mM solution, whereas cyanophenol-cyanophenol interactions are more likely for the 75 mM solution. Such differences in hydrogen bonding interactions should manifest as shifts in the frequency of the CN mode. However, ν_{CN} at the dilute concentration is identical to that at the higher concentration. For this reason we believe that dimerization at the air−water interface is unlikely and propose that the dominant interactions at the surface are between cyanophenol and water molecules.

Fitting the BBSFG spectra in Figure 2 also provides resonant amplitudes of the CN peak. This peak amplitude is found to increase with increasing solution concentration for both *m*-CP and *p*-CP. Since the sum-frequency spectral intensity depends on both the number of surface molecules as well as their orientation, a plot of SFG amplitude against the surface concentration of cyanophenol will be linear if the average orientation of the CN group does not change as a function of concentration. Figure 3 shows these plots for *m*-CP and *p*-CP at the air−water interface, and in both cases a linear relationship between SFG amplitude and surface concentration is evident. Thus, we conclude that the spectral increases shown in Figure 2 are due predominantly to enhanced surface coverage of the cyanophenols and not to changes in their molecular orientation. Interestingly, second harmonic generation (SHG) studies of another substituted phenol, *p*-nitrophenol, at the air−water interface also find that the molecular orientation remains constant over a wide range of surface concentrations.[40] The invariance of the cyanophenol orientation is, however, in stark contrast to SFG results for acetonitrile and long-chain alkyl nitriles in which the CN group changes from a more upright orientation at low surface concentration to an orientation closer to the surface plane at high concentration.[34,41]

Figure 4 shows BBSFG spectra of the CN stretching vibration taken under three polarization combinations, ssp, sps, and ppp. The ssp signal is the strongest for both isomers although the sps signal is also well above baseline noise. Significant peak asymmetry is evident in all polarization spectra, indicative of interference between resonant and nonresonant components of $\chi^{(2)}$. These polarization spectra are fit to eq 6 using the parameters obtained from globally fitting the cyanophenol concentration series. In the following sections we describe how these spectra are used to determine the molecular orientation of the cyanophenol isomers at the air−water interface.

4.3. Quantitative Analysis of Molecular Orientation. The vibrational normal mode involving the CN stretch is quite localized, with ~90% of the motion restricted to the cyano C and N atoms.[42,43] This mode is therefore well-approximated by $C_{\infty v}$ symmetry with three dominant elements of the molecular hyperpolarizability β, of which two are unique: the component with Raman polarizability and dipole moment derivatives parallel to the cyano bond axis, β_{ccc}, and that with polarizability derivative perpendicular to this axis, $\beta_{aac} = \beta_{bbc}$. We believe that this local-mode approach to the hyperpolarizability tensor elements is appropriate in this case because of the cylindrical symmetry of the CN group and the localization of this normal mode. However, for molecules in which this assumption is not valid, a more complete determination of the elements of β is necessary.[44] To proceed with analysis of the molecular orientation, we derive expressions for $\chi^{(2)}$ elements in terms of these β elements. For this, eq 5 may be expressed as

$$\chi_{ijk}^{(2)} = \frac{N}{\epsilon_0}\int_0^{2\pi}\int_0^{2\pi}\int_0^{\pi} f(\theta)\,\beta_{ijk}(\theta)\sin\theta\,\mathrm{d}\theta\,\mathrm{d}\phi\,\mathrm{d}\varphi \quad (9)$$

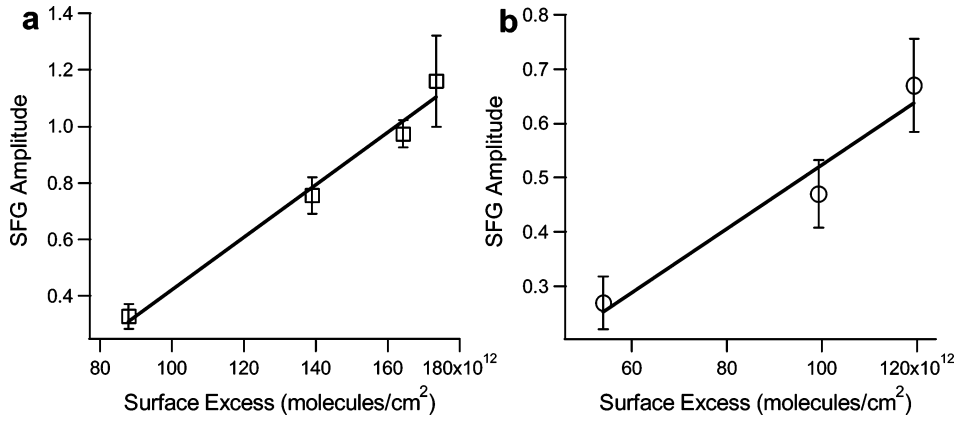

Figure 3. SFG fit amplitudes of the CN stretching vibration under ssp polarization as a function of surface excess for (a) *m*-cyanophenol and (b) *p*-cyanophenol at the air−water interface. The solid lines are linear fits to the data.

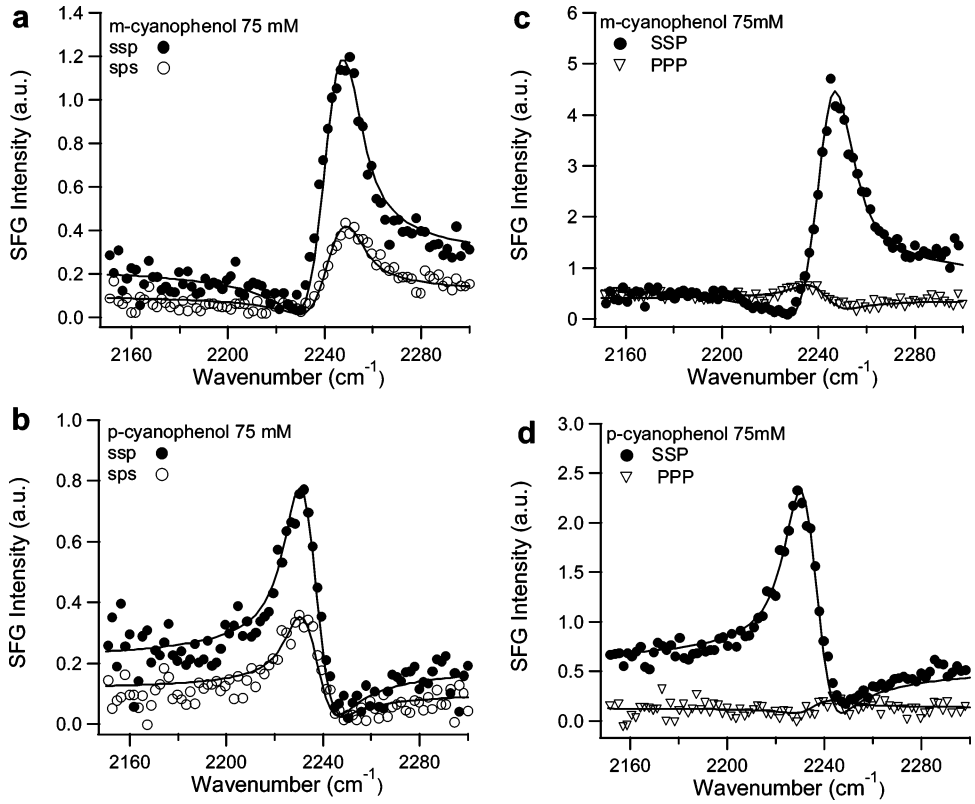

Figure 4. SFG spectra of the CN stretching vibration in three different polarization combinations: (a) *m*-cyanophenol in ssp and sps, (b) *p*-cyanophenol in ssp and sps, (c) *m*-cyanophenol in ssp and ppp, and (d) *p*-cyanophenol in ssp and ppp. Solid lines shown are fits to the data. Individual spectra in panels a and b were obtained in 10 min, while those in panels c and d were recorded in 20 min because of the relatively weaker ppp signal.

where elements of β have been transformed from the $lmn = abc$ molecular frame to the $ijk = xyz$ lab frame by projecting the cyano bond onto the surface normal, thereby defining the tilt angle θ.

$$\beta_{ijk}(\theta) = \sum_{lmn} U_{lmn:ijk}(\theta)\beta_{lmn} \tag{10}$$

There is no azimuthal orientation at a liquid surface and no twist angle about the cylindrically symmetric cyano bond, so the Euler angles ϕ and φ are uniformly distributed over 2π radians. The orientation distribution is then a function of the tilt angle only and is assumed to have either a delta

$$f(\theta) = c_N\delta(\theta - \theta_0) \tag{11}$$

or Gaussian form

$$f(\theta) = c_N \exp\left[\frac{(\theta - \theta_0)^2}{2\sigma^2}\right] \tag{12}$$

where θ_0 is the mean tilt angle and σ is the width of the angular distribution. c_N is a normalization constant defined such that

$$\int_0^{2\pi}\int_0^{2\pi}\int_0^{\pi} f(\theta)\sin\theta\,d\theta\,d\phi\,d\varphi = 1 \tag{13}$$

Spectra collected with the sps-polarization scheme probe the *yzy* element of $\chi^{(2)}$. Substituting the two unique β elements and performing the ϕ and φ integration results in

$$\chi_{yzy}^{(2)} = -\frac{N}{2\epsilon_0}\int_0^{\pi} f(\theta)\,\beta_{ccc}(r-1)\cos\theta\sin^2\theta\sin\theta\,d\theta \tag{14}$$

TABLE 2: Parameters Associated with the Sum-Frequency (SF), Visible, and IR Beams at the Air−Water Interface in the CN Stretching Region[a].

	m-cyanophenol			*p*-cyanophenol		
property	SF	visible	IR	SF	visible	IR
ω/cm^{-1}	14741	12500	2241	14736	12500	2236
γ/deg	57.2	60	45	57.2	60	45
n_{air}	1.0	1.0	1.0	1.0	1.0	1.0
n_{water}[b]	1.3295	1.3259	$1.3145 + 0.01171i$	1.3295	1.3259	$1.3142 + 0.01190i$
$n_{interface}$[c]	1.1484	1.1469	$1.1422 + 0.004896i$	1.1484	1.1469	$1.1420 + 0.004976i$
L_{xx}	1.038	1.066	$0.9522 - 0.002759i$	1.038	1.066	$0.9522 - 0.002759i$
L_{yy}	0.6878	0.6625	$0.7813 - 0.006307i$	0.6878	0.6625	$0.7813 - 0.006307i$
L_{zz}	0.7276	0.7063	$0.7923 + 0.002086i$	0.7276	0.7063	$0.7923 + 0.002086i$
$\hat{\mathbf{e}}_x$	$-\sin\gamma_{SF}$	$\sin\gamma_{vis}$	$\sin\gamma_{IR}$	$-\sin\gamma_{SF}$	$\sin\gamma_{vis}$	$\sin\gamma_{IR}$
$\hat{\mathbf{e}}_y$	1	1	1	1	1	1
$\hat{\mathbf{e}}_z$	$\cos\gamma_{SF}$	$\cos\gamma_{vis}$	$\cos\gamma_{IR}$	$\cos\gamma_{SF}$	$\cos\gamma_{vis}$	$\cos\gamma_{IR}$

[a] γ are the incident or reflected beam angles measured from the surface normal. [b] Bulk water refractive indices taken from ref 45. [c] Interfacial refractive indices calculated according to the model presented in ref 46.

where $r \equiv \beta_{aac}/\beta_{ccc}$. Similarly, spectra collected with the ssp-polarization scheme probe

$$\chi_{yyz}^{(2)} = \frac{N}{4\epsilon_0}\int_0^{\pi} f(\theta)\,\beta_{ccc}\cos\theta(1 + 3r + (r-1)\cos 2\theta)\sin\theta\,\mathrm{d}\theta \quad (15)$$

Finally, the ppp-polarization scheme probes four elements of $\chi^{(2)}$: *xxz*, *xzx*, *zxx*, and *zzz*. Therefore, eqs 14 and 15 may also be used to analyze the ppp data, along with the additional expression

$$\chi_{zzz}^{(2)} = \frac{N}{2\epsilon_0}\int_0^{\pi} f(\theta)\,\beta_{ccc}(r-1)\cos\theta\sin^2\theta\sin\theta\,\mathrm{d}\theta \quad (16)$$

The analysis then proceeds by taking ratios of the fit amplitudes obtained with different polarization schemes. The three amplitudes are used to construct two independent ratios

$$\frac{\chi_{eff,sps}^{(2)}}{\chi_{eff,ssp}^{(2)}} \quad \text{and} \quad \frac{\chi_{eff,ppp}^{(2)}}{\chi_{eff,ssp}^{(2)}} \quad (17)$$

When compared to analogous ratios constructed using eqs 14−16, the parameters θ_0 and σ in the orientation distribution functions may be obtained. These ratios eliminate the need to measure $\chi^{(2)}$ elements to absolute scale and do not require knowledge of the surface number density *N*. Furthermore, the quantity β_{ccc} disappears in the ratios, and so only the ratio of β elements, *r*, is required.

The effective susceptibilities defined in eq 2 require calculation of the Fresnel coefficients *L*, which in turn depend on refractive indices. We have used a three-phase model that requires nine complex refractive indices: those of the two bulk media (air and water)[45] and the interfacial region, each at the sum-frequency, visible, and infrared wavelength. The interfacial refractive index, n', has been calculated based on the two adjacent bulk phases according to the model presented by Zhuang et al.[46] Values of the refractive indices, unit polarization vectors, and Fresnel coefficients corresponding to our geometry appear in Table 2. In our analysis we have found that the orientation analysis is sensitive to the value of n' and the value of *r*, the ratio of dominant β elements; a more detailed discussion of this sensitivity follows in the Appendix.

The ratios in eq 17 were initially fit to a very narrow Gaussian (eq 12) or a delta distribution (eq 11), allowing the mean tilt angle and *r* to vary. This resulted in best-fit values of $r = 0.35$ for *m*-CP and $r = 0.23$ for *p*-CP. Subsequently holding these values of *r* fixed, slightly better fits could be obtained using a Gaussian distribution with adjustable mean tilt and distribution width. This resulted in the solutions $\theta_{mCP} = 74-84°$ (if $\chi^{(2)}_{NR} > 0$) or $180°-\theta_{mCP}$ (if $\chi^{(2)}_{NR} < 0$) and $\sigma_{mCP} < 10°$ for *m*-cyanophenol. For *p*-cyanophenol, the solutions are $\theta_{pCP} = 65-80°$ (if $\chi^{(2)}_{NR} < 0$) or $180°-\theta_{pCP}$ (if $\chi^{(2)}_{NR} > 0$) and $\sigma_{pCP} < 16°$. Given that the cyanophenols at the air−water interface are not likely to be well-ordered as in a densely packed monolayer, a Gaussian orientation distribution is a better approximation of the surface structure than a delta function. The ambiguity in the tilt angle of the CN group can be resolved if the sign of the nonresonant response is known.

4.4. Polarity of the Molecular Orientation. Since we do not measure the phase of the sum-frequency signal, we do not have a direct experimental measure of the absolute orientation of the cyano group. The spectral features reveal the relative phase between the resonant cyano mode and the nonresonant background. The absolute phase of the nonresonant and resonant response may, however, be shifted by 180°. In the present study we overcome this limitation by presenting an argument that reveals the sign of the nonresonant response, and therefore the absolute orientation for the para isomer.

The nonresonant contribution comes from two sources: water molecules and cyanophenol molecules at the surface. It has been demonstrated in experimental[47] and theoretical[48] studies that the nonresonant contribution at the neat air−water interface is negative in the ssp polarization scheme. Since $\chi^{(2)}_{NR,yyz} = \chi^{(2)}_{NR,yzy}$, we know that the nonresonant contribution from water in sps must also be negative. We have used ab initio methods to determine the relative magnitude and absolute sign for all elements of β_{NR} for the cyanophenol molecules. The nonresonant hyperpolarizability for both molecules is proportional to the static hyperpolarizability[48] and was determined using the Gaussian 03 package[49] with B3LYP[50] and the AUG-cc-pVDZ[51] basis set. Unlike the vibrational resonant response for the cyano mode, the electronic nonresonant response depends on the entire molecule, so we can no longer assume cylindrical symmetry about the cyano axis. We therefore assume a uniform distribution for azimuthal angles only, but consider the molecule aligned with a polar angle, θ_0, and a twist angle, ψ_0.

We first consider the para isomer, whose values of $\chi^{(2)}_{NR,yyz}$ are shown in Figure 5a. Analysis of the resonant CN mode has shown that the tilt angle is either in the range 65−80° or 100−115°, that is, pointing toward the vapor phase or away from it, respectively. Although the magnitude of the nonresonant response varies as the twist angle changes from 0 to 360°, for these tilt angles one can see that $\chi^{(2)}_{NR,yyz} > 0$ (solid contours)

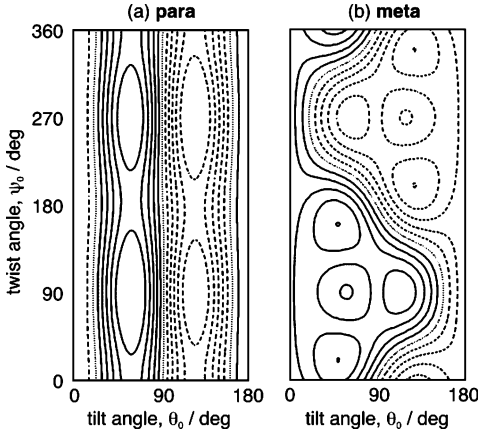

Figure 5. The nonresonant *yyz* element of $\chi^{(2)}$ for (a) *p*-cyanophenol and (b) *m*-cyanophenol. The mean tilt angle, θ_0, is defined between the surface normal (laboratory *z*-axis) and the cyano bond (molecular *c*-axis). The mean twist angle, Ψ_0, defines the molecule's orientation, rotated about the cyano bond. Solid contour lines indicate positive values of $\chi^{(2)}_{NR,yyz}$; dashed lines indicate negative values.

for $\theta_0 \approx 65-80°$, and $\chi^{(2)}_{NR,yyz} < 0$ (dashed contours) for $\theta_0 \approx 100-115°$. The fact that the variation in $\chi^{(2)}_{NR}$ is fairly small as the molecule is rotated about the cyano bond is reasonable for the *p*-CP since the electron density is roughly symmetrically distributed about this axis. If the cyano bond were pointing into the lower quadrant ($90° < \theta_0 < 180°$), the molecule's negative nonresonant response, combined with the negative nonresonant response of the water, would lead to an overall $\chi^{(2)}_{NR}$ (overall: cyanophenol + water) < 0. This contradicts the analysis that was presented for the resonant mode in section 4.3 (where the cyano group would be pointing into the top quadrant in the case of $\chi^{(2)}_{NR}$ (overall) < 0). We therefore rule out the possibility of this orientation. If the cyano group points into the top quadrant ($0° < \theta_0 < 90°$) however, Figure 5a shows that the nonresonant contribution from the cyanophenol is positive. This allows for the overall response to be negative (in the case where the $\chi^{(2)}_{NR}$ from water dominates the nonresonant response), consistent with analysis of the resonant mode. We therefore conclude that *p*-cyanophenol is oriented with $\theta_0 = 65-80°$ and that the surface water molecules dominate the nonresonant response.

Figure 5b shows that the analysis of *m*-cyanophenol is more complicated since $\chi^{(2)}_{NR}$ (cyanophenol) changes sign on the basis of the value of the twist angle. This result itself seems reasonable since rotating the molecule about the cyano axis causes the OH group, a major contributor to the molecule's polarizability and dipole moment, to reorient substantially. It is interesting to note that regardless of the quadrant in which the cyano group of the meta isomer points, it is reasonable to believe that the OH group will prefer to be directed toward the aqueous phase. Our choice of the molecular axes labels this orientation as one with ψ_0 in a broad range about 90° (as opposed to centered about 270° with the OH group in the air). Figure 5b shows that in a broad region about $\psi_0 = 90°$, either choice for the θ_0 quadrant would result in $\chi^{(2)}_{NR}$ (cyanophenol) > 0. If however, on the basis of our analysis of *p*-cyanophenol, we make use of the result that the nonresonant contribution is dominated by water, this results in $\chi^{(2)}_{NR}$ (overall) < 0, and on the basis of the analysis of the resonant mode in section 4.3, the assignment that the CN group of *m*-cyanophenol is oriented with $\theta_0 = 96-106°$. These orientations are illustrated in Figure 6. Thus, by deducing the sign of the overall nonresonant background we can resolve the ambiguity in the cyano tilt angle for *m*- and *p*-cyanophenol at the air−water interface and determine their absolute orientations.

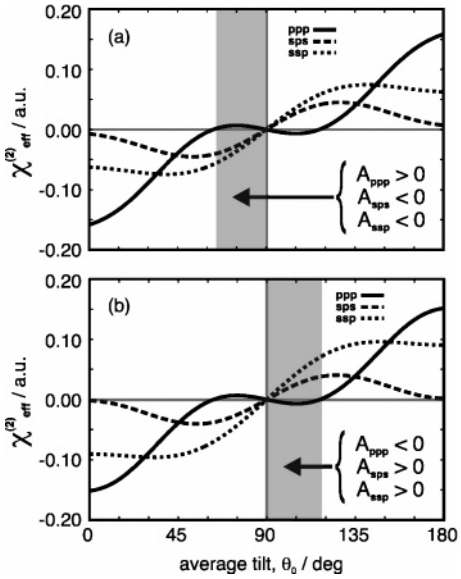

Figure 6. By deducing the sign of the nonresonant background to be negative for both isomers, the absolute orientation may be assigned. The shaded areas represent the range of tilt angles consistent with the observed resonant $\chi^{(2)}$ components. (a) In the case of *p*-cyanophenol $\theta_0 = 65-80°$, so the cyano bond points up toward the air. (b) For *m*-cyanophenol $\theta_0 = 96-106°$, so the cyano bond points down toward the aqueous phase.

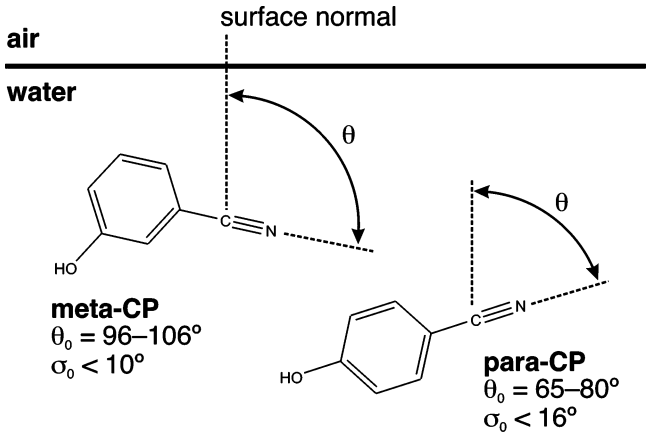

Figure 7. Illustration of the relative CN orientations of *m*-cyanophenol (left) and *p*-cyanophenol (right) at the air-water interface showing the average polar angle θ_0 and average Gaussian distribution width σ_0.

Discussion

One of the objectives of this study was to determine the influence of meta versus para substitution on the orientation of cyanophenol at the air−water interface. We have used vibrational sum-frequency spectra of the cyano mode to determine the orientation of the CN bond in *m*- and *p*-cyanophenol. Interestingly, our results show that the isomers adopt different orientations at the air−water interface. As depicted in Figure 7, on average, the CN group in *m*-CP points down ($\theta_0 \approx 96-106°$) into the aqueous bulk, while in *p*-CP the CN group points up ($\theta_0 \approx 65-80°$) toward the vapor phase. Although in both cases the cyano tilt angle lies close to the surface plane, the peak frequencies indicate that both CN groups are hydrogen bonded and so do not protrude out into the vapor phase. Moreover, the orientation analysis shows that this average tilt angle is distributed over a relatively narrow range, $\sigma < 10°$ for *m*-CP and $\sigma < 16°$ for *p*-CP. That this distribution width is slightly larger in the case of the para isomer may, in addition to a lower surface concentration, explain the weaker SFG

intensity observed for *p*-CP relative to *m*-CP at all bulk concentrations. The aromatic ring also likely has a preferred orientation with respect to the *z*-axis at the air−water interface, but without SFG spectra of the aromatic CH stretching modes, this orientation cannot be absolutely determined. Though we have obtained SFG spectra in this region, unambiguous mode assignment for each isomer is not possible.

The difference in CN orientation between *m*-and *p*-cyanophenol may arise from the relative hydrogen bonding strengths of the cyano and phenolic OH groups. For example, Raman spectra of benzonitrile in hydrogen-donating solvents such as phenol and methanol show, in addition to the CN stretching band of the monomer, a feature shifted by ∼6 to 9 cm^{-1} to higher frequency.[27,31] This additional band is attributed to the hydrogen-bonded complex between the CN group of benzonitrile and the hydroxyl group of either phenol or methanol. In contrast, laser-induced fluorescence studies of *o*-cyanophenol show that upon complexation with methanol, the phenolic OH group experiences a much more substantial red shift of ∼400 cm^{-1} with respect to free *o*-cyanophenol.[52] The modest CN frequency shift indicates that hydrogen bonds between water and the CN group of *m*- and *p*-cyanophenol are likely considerably weaker than those between water and the phenolic OH. These strong water-phenolic OH interactions may serve as a driving force for the overall orientations of these isomers at the air−water interface.

It is interesting to view the *p*-CP average tilt angle within the context of what is known about the interfacial orientation of two closely related compounds, benzene and phenol. In several experimental[53,54] and theoretical studies[55,56] of phenol at the air−water interface, it was shown that the most probable orientation is one in which the aromatic ring is perpendicular to the interface with the molecular long axis tilted ∼50° from the surface normal. In this orientation the hydroxyl group points down toward the water and part of the nonpolar ring protrudes into the vapor phase. In contrast, molecular dynamics simulations show that the absence of an OH substituent in benzene has a significant effect on its orientation at the same interface. Upon removal of the OH group the benzene ring reorients at the surface so that it is parallel to the surface (i.e., $\theta_0 \approx 90°$), thereby maximizing the van der Waals interactions between the solute and water.[56] Comparing these aromatic tilt angles with that of *p*-CP, we find that the *p*-cyanophenol angle ($\theta_0 \approx 65-80°$) is intermediate between the flat orientation of benzene and the near perpendicular orientation of phenol. Thus the *p*-cyanophenol orientation that we have determined is entirely reasonable given the requirement that both CN and OH groups are hydrogen bonded at the interface. Relative to phenol, the interaction between the cyano moiety and water increases the tilt of the aromatic ring orientation away from the surface normal.

The orientation of *m*-cyanophenol at the air−water interface is also determined by the balance of intermolecular interactions between hydrophobic and hydrophilic portions of the molecule and water. Unlike *p*-CP, however, in the case of *m*-CP the CN group tends to point down toward water. We propose that such an orientation not only allows solvation of both CN and OH substituents, but because of the meta substitution pattern, also readily enables a portion of the hydrophobic aromatic ring to protrude into the vapor phase.

Conclusions

A comprehensive study of the structure and orientation of *m*- and *p*-cyanophenol has been conducted using broad-bandwidth sum-frequency generation spectroscopy in combination with surface tension measurements. Surface tension and SFG experiments reveal that both isomers are surface active, though for the same bulk concentration, *m*-cyanophenol is present in slightly higher number at the interface than *p*-cyanophenol. We have also shown that the cyano group of both isomers is hydrogen bonded at the interface and therefore is not protruding into the vapor phase. Furthermore, SFG spectra of the CN stretching mode in different polarization schemes have been used to quantitatively determine the CN average tilt angle, θ_0, as well as the average angular distribution width, σ_0. Our analysis reveals that the orientation of both isomers does not change with surface density. However, we find that the cyano groups adopt different average orientations at the air−water interface such that in the case of *m*-cyanophenol the CN group tilts down toward the aqueous phase, but tilts up toward the vapor phase for *p*-cyanophenol. The average cyano tilt angle in both cases lies relatively close to the surface plane and is narrowly distributed, although the width of the angular distribution is slightly larger for *p*-cyanophenol. While the aromatic ring orientation was not directly determined, we infer that the shallow cyano tilt angle would enable the hydrophobic ring portions of both isomers greater access to the water surface.

The results reported here for *m*- and *p*-cyanophenol could have implications for the fate of halobenzonitrile pesticides in the environment. Such pesticides are primarily degraded in the atmosphere through direct photolysis and photooxidative reactions with OH radical or ozone. The surface adsorption and orientation of the cyanophenol isomers determined in this study indicate that heterogeneous reactions with oxidative species at the air−water interface could be an important pathway for their removal from the atmosphere.

Acknowledgment. The authors gratefully acknowledge the support of the National Science Foundation for this work. They would also like to thank Dr. Bruce Chase of DuPont for his Raman measurements and for his ongoing interest and helpful discussions.

Appendix

In our analysis, we have observed that the average tilt angle, θ_0, is very sensitive to the choice of n', the interfacial index of refraction. However, since the precise refractive index of the interfacial layer is often unknown, a number of approaches have been used to estimate its value. Many researchers adopt a two-phase model in which n' equals either of the bulk phase indices of refraction. However, it is not always clear which bulk index should be used. Zhuang and co-workers for example, found that assuming a two-phase model produced unreasonable results in their analysis of the orientation of pentyl cyanoterphenyl molecules at the air−water interface.[46] Upon adopting a three-phase model for the interface in which n' is calculated on the basis of estimates of local field corrections at the interface, however, these difficulties were resolved.[46] This suggests that the value of n' used in the analysis of SFG data needs to be considered with care and that it may not correspond simply to the refractive index of one of the bulk phases at the interface. Like Zhuang and co-workers, we initially adopted a two-phase interfacial model in our analysis of the cyanophenol orientation but found that it did not yield any agreement between experimental and calculated $\chi^{(2)}$ ratios (eq 17). As a result, we used a three-phase model for the interface [45] which gave $n' \approx 1.15$.

Using this value for n', the values of r for *m*-CP (0.35) and *p*-CP (0.23) determined from the data analysis are in good

agreement with those derived from other SFG studies of monolayers of long-chain cyano compounds at the air−water interface.[41,46] As in the present study, these works quantitatively determined the orientation of the CN headgroup. In both cases, the authors deduced the value of r for the cyano mode from an orientation analysis done in a similar way to that presented here, and found $r = 0.26$ and $r = 0.25 \pm 0.03$. Another widely used approach is to deduce r from Raman measurements of the depolarization ratio, ρ, which can be related to r. Our gas-phase calculations of the depolarization ratio yields $r = 0.07$ for *m*-CP and $r = 0.05$ for *p*-CP. These values of r are significantly different from those deduced from our SFG data, and attempts to use them in the orientation analysis resulted in no agreement between calculated and experimental $\chi^{(2)}$ ratios, regardless of the value of n'.

This discrepancy between estimates of r based on Raman depolarization ratios versus analysis of SFG data could stem from the sensitivity of β to molecular environment. The Gaussian calculations above yield gas-phase values which clearly do not reflect the hydrogen-bonding environment of the cyanophenol isomers. Such sensitivity of β has been nicely illustrated in a recent SFG experiment by Hommel et al. of the air−liquid benzene interface.[57] The strong CH stretching signal observed from the neat benzene surface is an unexpected result given that benzene is centrosymmetric, and therefore β is calculated to be zero. The authors suggest that distortion to the benzene electron density arising from the anisotropy of the interface results in a perturbation of the hyperpolarizability from the local environment, and hence a nonzero interfacial $\chi^{(2)}$ response.

References and Notes

(1) Costanza, M. S.; Brusseau, M. L. *Environ. Sci. Technol.* **2000**, *34*, 1.
(2) Lenhart, J. J.; Saires, J. E. *Environ. Sci. Technol.* **2004**, *38*, 120.
(3) Seinfeld, J. H.; Pankow, J. F. *Ann. Rev. Phys. Chem.* **2003**, *54*, 121.
(4) Molina, M. J.; Ivanov, A. V.; Trakhtenberg, S.; Molina, L. T. *Geophys. Res. Lett.* **2004**, *31*, L22104.
(5) Rudich, Y. *Chem. Rev.* **2003**, *103*, 5097.
(6) Georgieva, M. K.; Angelova, P. N.; Binev, I. G. *J. Mole. Struct.* **2004**, *692*, 23.
(7) Millet, M.; Palm, W.-U.; Zetzsch, C. *Ecotoxicol. Environ. Saf.* **1998**, *41*, 44.
(8) Palm, W.-U.; Millet, M.; Zetzsch, C. *Ecotoxicol. Environ. Saf.* **1998**, *41*, 36.
(9) Vieceli, J.; Roeselova, M.; Potter, N.; Dang, L. X.; Garrett, B. C.; Tobias, D. J. *J. Phys. Chem. B* **2005**, *109*, 15876.
(10) McCarley, K. D.; Bunge, A. L. *Int. J. Pharm.* **2003**, *250*, 169.
(11) Swiek, B. *Zesz. Nauk. Uniw. Jagiellon., Pr. Chem.* **1971**, *16*, 79.
(12) Shen, Y. R. *The Principles of Nonlinear Optics*; John Wiley & Sons: New York, 1984.
(13) Richmond, G. L. *Chem. Rev.* **2002**, *102*, 2693.
(14) Eisenthal, K. B. *Chem. Rev.* **1996**, *96*, 1343.
(15) Bell, G. R.; Bain, C. D.; Ward, R. N. *J. Chem. Soc., Faraday Trans.* **1996**, *92*, 515.
(16) Knock, M. M.; Bain, C. D. *Langmuir* **2000**, *16*, 2857.
(17) Watry, M. R.; Richmond, G. L. *J. Am. Chem. Soc.* **2000**, *122*, 875.
(18) Brown, M. G.; Raymond, E. A.; Allen, H. C.; Scatena, L. F.; Richmond, G. L. *J. Phys. Chem. A* **2000**, *104*, 10220.
(19) Hirose, C.; Akamatsu, N.; Domen, K. *Appl. Spectrosc.* **1992**, *46*, 1051.
(20) Rame, E. *J. Colloid Interface Sci.* **1997**, *185*, 245.
(21) Richter, L. J.; Petralli-Mallow, T. P.; Stephenson, J. C. *Optics Lett.* **1998**, *23*, 1594.
(22) Bain, C. D.; Davies, P. B.; Ong, T. H.; Ward, R. N. *Langmuir* **1991**, *7*, 1563.
(23) Goates, S. R.; Schofield, D. A.; Bain, C. D. *Langmuir* **1999**, *15*, 1400.
(24) Moore, F. G.; Becraft, K. A.; Richmond, G. L. *Appl. Spectrosc.* **2002**, *56*, 1575.
(25) Rosen, M. J. *Surfactants and Interfacial Phenomena*; John Wiley & Sons: New York, 1978.
(26) Johnson, C. M.; Tyrode, E.; Baldelli, S.; Rutland, M. W.; Leygraf, C. *J. Phys. Chem.* B **2005**, *109*, 329.
(27) Abramczyk, H.; Reimschussel, W. *Chem. Phys.* **1985**, *100*, 243.
(28) Marcus, Y. *J. Phys. Org. Chem.* **2003**, *16*, 398.
(29) Matos, M. A. R.; Miranda, M. S.; Morais, V. M. F. *Struct. Chem.* **2004**, *15*, 103.
(30) Reimers, J. R.; Hall, L. E. *J. Am. Chem. Soc.* **1999**, *121*, 3730.
(31) Bhriguvansh, P. R. n.; Srivastava, S. K.; Singh, R. K.; Asthana, B. P.; Kiefer, W. *Phys. Chem. Chem. Phys.* **2004**, *6*, 531.
(32) Getahun, Z.; Huang, C.-Y.; Wang, T.; Leon, B. D.; DeGrado, W. F.; Gai, F. *J. Am. Chem. Soc.* **2003**, *125*, 405.
(33) Chaban, G. M. *J. Phys. Chem. A* **2004**, *108*, 4551.
(34) Zhang, D.; Gutow, J. H.; Eisenthal, K. B. *J. Chem. Phys.* **1993**, *98*, 5099.
(35) Bernstein, M. P.; Sandford, S. A.; Allamandola, L. J. *Astrophys. J.* **1997**, *476*, 932.
(36) Mollner, A. K.; Brooksby, P. A.; Loring, J. S.; Bako, I.; Palinkas, G.; Fawcett, W. R. *J. Phys. Chem. A* **2004**, *108*, 3344.
(37) Exner, O.; Bocek, K. *Collect. Czech. Chem. Commun.* **1973**, *38*, 50.
(38) Chase, B. *Raman Spectra of meta- and para- Cyanophenol*; Dupont: St. Petersburg, FL, 2005.
(39) Higashi, T.; Osaki, K. *Acta Crystallogr. B* **1977**, *133*, 607.
(40) Higgins, D. A.; Abrams, M. B.; Byerly, S. K.; Corn, R. M. *Langmuir* **1992**, *8*, 1994.
(41) Zhang, D.; Gutow, J.; Eisenthal, K. B. *J. Phys. Chem.* **1994**, *98*, 13729.
(42) Andrews, S. S.; Boxer, S. G. *J. Phys. Chem. A* **2000**, *104*, 11853.
(43) Binev, Y. I. *J. Mole. Struct.* **2001**, *535*, 93.
(44) Hore, D. K.; Beaman, D. K.; Parks, D. H.; Richmond, G. L. *J. Phys. Chem. B* **2005**, *109*, 16846.
(45) Segelstein, D. J. *The Complex Refractive Index of Water*; University of Missouri: Kansas City, MO, 1981.
(46) Zhuang, X.; Miranda, P. B.; Kim, D.; Shen, Y. R. *Phys. Rev. B: Condens. Matter Mater. Phys.* **1999**, *59*, 12632.
(47) Raymond, E. A.; Tarbuck, T. L.; Brown, M. G.; Richmond, G. L. *J. Phys. Chem. B* **2003**, *107*, 546.
(48) Morita, A.; Hynes, J. T. *J. Phys. Chem. B* **2002**, *106*, 673.
(49) Frisch, M. J.; Trucks, G. W.; Schlegel, H. B.; Scuseria, G. E.; Robb, M. A.; Cheeseman, J. R.; Montgomery, J. A., Jr.; Vreven, T.; Kudin, K. N.; Burant, J. C.; Millam, J. M.; Iyengar, S. S.; Tomasi, J.; Barone, V.; Mennucci, B.; Cossi, M.; Scalmani, G.; Rega, N.; Petersson, G. A.; Nakatsuji, H.; Hada, M.; Ehara, M.; Toyota, K.; Fukuda, R.; Hasegawa, J.; Ishida, M.; Nakajima, T.; Honda, Y.; Kitao, O.; Nakai, H.; Klene, M.; Li, X.; Knox, J. E.; Hratchian, H. P.; Cross, J. B.; Bakken, V.; Adamo, C.; Jaramillo, J.; Gomperts, R.; Stratmann, R. E.; Yazyev, O.; Austin, A. J.; Cammi, R.; Pomelli, C.; Ochterski, J. W.; Ayala, P. Y.; Morokuma, K.; Voth, G. A.; Salvador, P.; Dannenberg, J. J.; Zakrzewski, V. G.; Dapprich, S.; Daniels, A. D.; Strain, M. C.; Farkas, O.; Malick, D. K.; Rabuck, A. D.; Raghavachari, K.; Foresman, J. B.; Ortiz, J. V.; Cui, Q.; Baboul, A. G.; Clifford, S.; Cioslowski, J.; Stefanov, B. B.; Liu, G.; Liashenko, A.; Piskorz, P.; Komaromi, I.; Martin, R. L.; Fox, D. J.; Keith, T.; Al-Laham, M. A.; Peng, C. Y.; Nanayakkara, A.; Challacombe, M.; Gill, P. M. W.; Johnson, B.; Chen, W.; Wong, M. W.; Gonzalez, C.; Pople, J. A. *Gaussian 03*, revision C.02; Gaussian, Inc.: Wallingford, CT, 2004.
(50) Becke, A. D. *J. Chem. Phys.* **1993**, *98*, 5648.
(51) Dunning, T. H. *J. Chem. Phys.* **1989**, *90*, 1007.
(52) Broquier, M.; Lahmani, F.; Zehnacker-Rentien, A.; Brenner, V.; Millie, P.; Peremans, A. *J. Phys. Chem. A* **2001**, *105*, 6841.
(53) Kemnitz, K.; Bhattacharyya, K.; Hicks, J. M.; Pinto, G. R.; Eisenthal, K. B.; Heinz, T. F. *Chem. Phys. Lett.* **1986**, *131*, 285.
(54) Hicks, J. M.; Kemnitz, K.; Eisenthal, K. B. *J. Phys. Chem.* **1986**, *90*, 560.
(55) Sokhan, V. P.; Tildesley, D. J. *Faraday Discuss.* **1996**, *104*, 193.
(56) Pohorille, A.; Benjamin, I. *J. Chem. Phys.* **1991**, *94*, 5599.
(57) Hommel, E. L.; Allen, H. C. *Analyst* **2003**, *128*, 750.